Conical Electrostatic Probe Response in a Weakly Ionized Gas Flow

C.F. Bruce* and L. Talbot†
University of California, Berkeley, Calif.

The current-voltage characteristics of conical electrostatic probes were measured in a partially ionized argon flow over the range of ion number density 10^8-10^{13} cm^{-3}. The characteristics were compared to theoretical predictions of various thin and thick-sheath theories, including the Stahl and Su theory, modified for the conical geometry. No theory gave completely satisfactory predictions, but the thin-sheath theories, when modified to include a dependence of the current on the square root of the probe voltage, were somewhat more satisfactory than the thick-sheath ones.

Nomenclature

A_p = probe area, cm^2
D = diffusion coefficient, cm^2/sec
e = charge on electron, coulombs
$f(\eta)$ = Blasius stream function, $(2u_\infty \nu_\infty x)^{-1/2}\psi$
h = enthalpy
$I(r)$ = current density, amps/cm^2
I_p = probe current, amps
k = Boltzman constant
L, L_p = probe length along centerline
L_s = probe length along surface
M = Mach number
n = number density, cm^{-3}
p = pressure, Torr
p_0 = stagnation pressure
$\bar{Q}$ = heat flux
$\bar{q}$ = velocity vector
Re = Reynolds number
r = radial position
Sc^i = ion Schmidt number, ν/D^i
T = temperature, Kelvin
T_o = stagnation temperature
u = velocity in x- or r-direction
V, V_p, V_c = probe potential, volts
v = velocity in the y- or θ-direction
x, y = cartesian coordinates
γ = ratio of specific heats
θ = angular position
θ_b = matching position between sheath and quasi-neutral regions
θ_0 = cone half angle
λ_D = Debye length, $6.92(T^e/n^e)^{1/2}$, cm, T^e ,in Kelvin, n^e in cm^{-3}
$\lambda_{\alpha\beta}$ = mean free path for species α and β
ν = kinematic viscosity, μ/ρ
ρ = density
τ = stess tensor
Φ = viscous dissipation function
ϕ = probe potential, volts

Subscripts

c = refers to properties of inviscid flow at cone surface
w = refers to probe surface
∞ = refers to properties of freestream

Superscripts

e = refers to electrons
i = refers to ions

Introduction

TO characterize flows such as flames, rocket exhausts, or flows that occur on bodies moving at high speed in the earth's atmosphere, the local ionized gas properties, electron temperature, and ion number density must be determined. One widely used method for measuring these properties is to calculate them from measured current-voltage characteristics (probe responses) of electrostatic probes.[1]

The theoretical relationships between the current-voltage characteristics and the electrical properties of the gas are simplest for probes of cylindrical and spherical geometry, but the use of these geometries is often precluded by the hostile environment presented by a high-temperature flow. On the other hand, a slender conical probe shape provides the sturdy structure and the ability to absorb a high rate of heat transfer required by these applications.

The disadvantage in the use of conical probes is that the theory necessary to interpret their response is less developed than for cylindrical or spherical probes, and in particular if small conical probes are used to improve spatial resolution in flow measurements, the situation can arise where the region of electrical influence of the probe (the probe sheath) can extend out beyond the region of fluid-dynamical influence. This domain of probe operation is not well-understood on a theoretical basis.

The purpose of this investigation was to measure the current-voltage characteristics of conical electrostatic probes in continuum flows with a wide ion density range and correspondingly wide sheath thickness range, and to compare these characteristics with those predicted by thin and thick-sheath theories in order to study their utilization in the measurement of ion densities.

Several theoretical studies have been made of probes with sheath thicknesses much larger than the boundary layers.[2-6] Of these so-called thick-sheath theories, only the paper by Hammitt[4] was in the proper form for direct comparison with the measurements because of the restrictive assumptions and geometries.

Presented as Paper 75-179 at the AIAA 13th Aerospace Sciences Meeting, Pasadena, Calif., January 20-22, 1975; submitted January 27, 1975; revision received May 22, 1975. This research was supported by the Air Force Office of Scientific Research. The authors would like to thank Professors F. Robben and D. R. Willis for their contributions to this work.

Index categories: Plasma Dynamics and MHD; Atomic, Molecular and Plasma Properties.

*Research Assistant; presently Staff Member, MIT Lincoln Laboratory, Lexington, Massachusetts. Member AIAA.

†Professor. Member AIAA.

Sheaths much thinner than the boundary layer thickness were considered in theories by Chung and Blankenship[7] and Denison.[8] They derived expressions directly relating ion density to conical probe ion saturation current.

Moderately thin sheaths, of boundary layer size, have been treated by Baum and Denison[9] and Stahl and Su.[10] The Stahl and Su theory yields typical current-voltage characteristics of flat-plate flush probes for both uniform and Blasius boundary layer models of the neutral species flow. In the other analyses referred to, current-voltage characteristics were not calculated.

In the following study we first present a theoretical treatment of conical probe response based on the formulation of Stahl and Su. In the subsequent sections the experimental work is described, and comparisons with the several theories mentioned are made.

Theory

The equations used to model the flow are the incompressible momentum and continuity equations for singly charged ions and electrons and Poisson's equation (assuming $T^i = T^e = T$).

$$\nabla \cdot [\bar{q}\, n^i - D^i \nabla n^i - (eD^i/kT) n^i \nabla \phi] = 0$$

(ion continuity and momentum)

$$\nabla \cdot [\bar{q}\, n^e - D^e \nabla n^e + (eD^e/kT) n^e \nabla \phi] = 0$$

(electron continuity and momentum)

$$\nabla^2 \phi = -4\pi e (n^i - n^e)$$

(Poisson's equation)

The following analysis considers the conical probe geometry (see Fig. 1). It is based on the thin-sheath theory, which Stahl and Su[10] proposed and applied to the flat-plate flush probe. The flowfield is divided into two regions: a quasi-neutral region in which it is assumed that ion and electron densities are equal, and a sheath near the probe surface where the charge separation occurs.

For conical geometry we use spherical polar coordinates r and θ, and we first consider the sheath region. We assume axisymmetric flow with $n_\infty = n_\infty{}^i = n_\infty{}^e$, and we introduce the following nondimensional variables:

$$r^* = r/L, \qquad \theta^* = (u_\infty r/D^i)^{1/2}\theta, \qquad n_i^* = n^i/n_\infty$$

$$\phi^* = e\phi/kT, \quad u^* = u/u_\infty, \qquad v^* = (r/D^i u_\infty)^{1/2} v$$

The subscript ∞ denotes the value of the variable at the outer limit of the sheath. If it is reasonable to assume that the sheath is thin so that $\sin\theta \approx \sin\theta_0$ and that $u_\infty L/D^i \gg 1$, then we can write the three equations (retaining only normal derivatives of n_i and ϕ^*) as

$$(\mathrm{d}/\mathrm{d}\theta^*)(n_i^* v^*) = \mathrm{d}^2 n_i^*/\mathrm{d}\theta^{*2} + (\mathrm{d}/\mathrm{d}\theta^*)(n_i^* \mathrm{d}\phi^*/\mathrm{d}\theta^*)$$

$$(\mathrm{d}/\mathrm{d}\theta^*)(n_e^* v^*) = \mathrm{d}^2 n_e^*/\mathrm{d}\theta^{*2} - (\mathrm{d}/\mathrm{d}\theta^*)(n_e^* \mathrm{d}\phi^*/\mathrm{d}\theta^*)$$

and

$$\mathrm{d}^2\phi^*/\mathrm{d}\theta^{*2} = (D^i r/\lambda_D{}^2 u_\infty)(n_i^* - n_e^*)$$

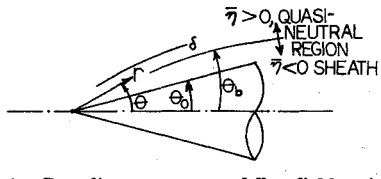

Fig. 1 Coordinate system and flowfield regions.

Now if $-\phi^* \gg 1$, we can neglect the electron current reaching the probe surface. Integrating the electron continuity-momentum equation from the surface to the sheath gives

$$\mathrm{d}n_e^*/\mathrm{d}\theta^* - n_e^* \mathrm{d}\phi^*/\mathrm{d}\theta^* = 0$$

We can integrate again to obtain

$$n_e^* = \exp(\phi^*)$$

The conservation equation for ions can be integrated yielding

$$\mathrm{d}n_i^*/\mathrm{d}\theta^* + n_i^*\, \mathrm{d}\phi^*/\mathrm{d}\theta^* = -n_{i_w}{}^* v_w^* \equiv I^+$$

At the inner limit of the quasineutral region, we use the usual boundary condition, $n_i^* \to 0$. In order to match the sheath solutions to this behavior, we require the dependence of n_i^* on θ^* to be that of a first-order Taylor series, that is, for the sheath outer boundary condition we take $n_i^* \approx A(\theta^* - \theta_b^*)$ where $A = (\mathrm{d}n_i^*/\mathrm{d}\theta^*)$ and the subscript b denotes the value of the variable at the outer limit of the sheath (also the inner limit of the quasi-neutral region). Since the sheath is thin, for its analysis we introduce a small parameter ϵ, and we stretch the variables by setting

$$\eta = (A/\epsilon)(\theta^* - \theta_b^*), \qquad N = n_i^*/\epsilon, \qquad \text{and} \qquad \psi = \phi^* - \ln \epsilon$$

Note that ψ is a negative quantity and η is negative within the sheath. The ion equation becomes

$$\mathrm{d}N/\mathrm{d}\eta + N(\mathrm{d}\psi/\mathrm{d}\eta) = I^+/A$$

and Poisson's equation becomes

$$\mathrm{d}^2\psi/\mathrm{d}\eta^2 = (\epsilon^3 D^i r/A^2 \lambda_D{}^2 u_\infty)(N - e^\psi)$$

This form of Poisson's equation indicates that the choice of ϵ should be

$$\epsilon \equiv (A^2 \lambda_D{}^2 u_\infty / D^i r)^{1/3}$$

The boundary conditions at the wall $\eta = \eta_0$ are

$$N(\eta = \eta_0) = 0$$

$$\psi(\eta = \eta_0) = \phi_p^* - \ln \epsilon$$

At the outer boundary of the sheath region, the boundary conditions are

$$n_i^*(\theta_b^*) = (\mathrm{d}n_i^*/\mathrm{d}\theta^*)(\theta^* - \theta_b^*) \Rightarrow N(\eta \to \eta_b) \to \eta(\mathrm{d}N/\mathrm{d}\eta),$$

$$\psi(\eta \to \eta_b) \to \ln N \to \ln \eta$$

Now the governing differential equations and boundary conditions are identical to those of Stahl and Su. Hence their numerical solution for $\psi_p(\eta_0)$ can be used directly, where

$$\psi_p(\eta_0) = e\phi_p/kT - \ln[(J/2)^{2/3}\lambda_D^2] \tag{1}$$

and

$$\eta_0 = -(J/2)^{1/3} r(\theta_b - \theta_0) \tag{2}$$

The subscript 0 denotes the value of the variable at the cone surface, J is given by

$$J \equiv (2A/\lambda_D{}^2)(u_\infty/D^i r)^{1/2}$$

and $I^+ = 2A$. The expression for ψ_p still includes the quantity A, which we must relate to the neutral flow properties by con-

sidering the boundary layer on the cone and the quasi-neutral region.

The neutral flow continuity, momentum, and constant pressure energy equations are written

$$\partial\rho/\partial t + \nabla\cdot(\rho\bar{q}) = 0$$

$$\rho(\partial\bar{q}/\partial t) + \rho\bar{q}\cdot\nabla\bar{q} + \nabla p = \text{div } \underline{\underline{\tau}}$$

$$\rho(\partial h/\partial t) + \rho\bar{q}\cdot\nabla h = \Phi - \text{div } \bar{Q}$$

Assume that for the boundary layer $u_\infty r/\nu_\infty \gg 1$, $\sin\theta \approx \sin\Theta_0$, and that the flow is steady. Then the three above equations can be written

$$(\partial/\partial r)\ (\rho u) + 2\rho u/r + (1/r)\ (\partial/\partial\theta)\ (\rho v) = 0$$

$$\rho[u(\partial u/\partial r) + (v/r)\ (\partial u/\partial\theta)] = (1/r^2)\ (\partial/\partial\theta)\ [\mu(\partial u/\partial\theta)]$$

and

$$\rho\left(u\frac{\partial h}{\partial r} + \frac{v}{r}\frac{\partial h}{\partial\theta}\right) = \frac{\mu}{r^2}\left(\frac{\partial u}{\partial\theta}\right)^2 + \frac{1}{r^2}\frac{\partial}{\partial\theta}\left(\frac{k}{c_p}\frac{\partial h}{\partial\theta}\right)$$

Following the analysis of Hantzsche and Wendt,[11] we assume u and h are functions of one independent variable, $\bar{\eta}$. We define $\bar{\eta}$ and v_c as follows:

$$\bar{\eta} \equiv (3u_\infty r/2\nu_\infty)^{1/2}(\theta - \theta_0)$$

$$v_c \equiv (2/3)\bar{\eta}u_\infty + (u_\infty r/6\nu_\infty)^{1/2} v$$

Then the three boundary-layer equations reduce to

$$-(\bar{\eta}/2)\ (\mathrm{d}/\mathrm{d}\bar{\eta})\ (\rho u) + (\mathrm{d}/\mathrm{d}\bar{\eta})\ (\rho v_c) = 0$$

$$(2\nu_\infty/u_\infty)[(-\rho u\bar{\eta}/2) + \rho v_c]\,\mathrm{d}u/\mathrm{d}\bar{\eta} = (\mathrm{d}/\mathrm{d}\bar{\eta})\ (\mu\,\mathrm{d}u/\mathrm{d}\bar{\eta})$$

and

$$(2\nu_\infty/u_\infty)[(-\rho u\bar{\eta}/2) + \rho v_c]\,\mathrm{d}h/\mathrm{d}\bar{\eta} = (\mathrm{d}/\mathrm{d}\bar{\eta})\ [(k/c_p)\ (\mathrm{d}h/\mathrm{d}\bar{\eta})] + \mu(\mathrm{d}u/\mathrm{d}\bar{\eta})^2$$

The boundary conditions at the cone surface are

$$u(\bar{\eta}=0) = 0 \quad \text{and} \quad v_c(\bar{\eta}=0) = 0 \quad (\text{because } v=0)$$

At the outer edge of the boundary layer

$$u(\bar{\eta}\to\infty)\to u_\infty, \quad v(\bar{\eta}\to\infty)\to 0, \quad \text{and } h(\bar{\eta}\to\infty)\to h_\infty$$

The above equations and boundary conditions are identical to those for a flat plate if $\bar{\eta}$, $u(\bar{\eta})$, $v_c(\bar{\eta})$, and $h(\bar{\eta})$ are replaced by

$$\eta_1 = \sqrt{u_\infty/2\nu_\infty x}\ y,\ u(\eta_1), v_{\text{f.p.}} = \sqrt{u_\infty x/2\nu_\infty}\, v(\eta_1),$$

and $h(\eta_1)$, respectively.

To model the physical flow under consideration we assume $T_w = T_\infty$. (In the experiment to be discussed subsequently, the probes were water-cooled and the temperature of the flow at the nozzle exit was near to room temperature.) Also, as shown in Schlichting,[12] Fig. 13.11, the maximum temperature within the boundary layer for $M_\infty = 2.16$ is only about 20% larger than the wall or freestream temperature. Since the pressure is assumed constant across the boundary layer, the density can vary by only about 20%, and the flat-plate boundary layer is not badly modeled by that of an incompressible flow. Therefore we set $u = u_\infty f'(\bar{\eta})$ and $v_c = (u_\infty/2)[\bar{\eta}f'(\bar{\eta}) - f(\bar{\eta})]$, where $f(\bar{\eta})$ is the solution to the Blasius equation $f''' + ff'' = 0$ (see, e.g., Rosenhead,[13] Table V.1), and we drop the energy equation altogether.

In the quasineutral region the conservation equations for ions and electrons are (assuming $n \equiv n^i = n^e$)

$$\nabla\cdot[\bar{q}n - D^i\nabla n - (eD^i/kT)n\nabla\phi] = 0$$

and

$$\nabla\cdot[\bar{q}n - D^e\nabla n + (eD^e/kT)n\nabla\phi] = 0$$

We divide each equation by its diffusion coefficient and add the two equations to obtain

$$[(D^i + D^e)/2D^iD^e]\,\nabla\cdot\bar{q}n = \nabla^2 n$$

which becomes (using axisymmetric, spherical polar coordinates and the boundary-layer assumptions, together with the neutral gas incompressibility and charge neutrality conditions)

$$[(D^i + D^e)/2D^iD^e]\,(u\partial n/\partial r + v\partial n/\partial\theta) = (1/r^2)\,(\partial^2 n/\partial\theta^2)$$

We use the formulation in terms of $\bar{\eta}$ as before, and simplify by assuming

$$\nu_\infty(D^i + D^e)/2D^iD^e \approx \nu_\infty/2D^i = 1$$

The resulting equation for $n(\bar{\eta})$ is

$$\mathrm{d}^2 n/\mathrm{d}\bar{\eta}^2 + f(\bar{\eta})\,\mathrm{d}n/\mathrm{d}\bar{\eta} = 0$$

with boundary conditions

$$n(\bar{\eta}_b) = 0 \quad \text{and} \quad n(\bar{\eta}\to\infty)\to n_\infty$$

The solution can be written as (with primes denoting differentiation with respect to $\bar{\eta}$)

$$n/n_\infty = 1 - [(1 - f'(\bar{\eta}))/(1 - f'(\bar{\eta}_b))]$$

Hence

$$\frac{1}{n_\infty}\left(\frac{\mathrm{d}n}{\mathrm{d}\bar{\eta}}\right)_b = \frac{f''(\bar{\eta}_b)}{1 - f'(\bar{\eta}_b)} = \frac{1}{n_\infty}\left(\frac{2\nu_\infty}{3u_\infty r}\right)^{1/2}\left(\frac{\mathrm{d}n}{\mathrm{d}\theta}\right)_b$$

or

$$\left(\frac{\mathrm{d}n}{\mathrm{d}\theta}\right)_b = n_\infty\left(\frac{3u_\infty r}{2\nu_\infty}\right)^{1/2}\left[\frac{f''(\bar{\eta}_b)}{1 - f'(\bar{\eta}_b)}\right]$$

Thus

$$A \equiv \left(\frac{\mathrm{d}n^*}{\mathrm{d}\theta^*}\right)_b = \frac{\sqrt{3}}{2}\left[\frac{f''(\bar{\eta}_b)}{1 - f'(\bar{\eta}_b)}\right]$$

and

$$J = \frac{1}{\lambda_D{}^2}\left(\frac{6u_\infty}{\nu_\infty r}\right)^{1/2}\left[\frac{f''(\bar{\eta}_b)}{1 - f'(\bar{\eta}_b)}\right] \tag{3}$$

where

$$\bar{\eta}_b = \left(\frac{3u_\infty r}{2\nu_\infty}\right)^{1/2}(\theta_b - \theta_0) \tag{4}$$

The probe current is given by

$$I_p = \int I(r)\,\mathrm{d}A = \int_0^{L/\cos\theta_0} I(r)\,2\pi r\sin\theta_0\,\mathrm{d}r$$

where

$$I(r) = I^+ e\, n_\infty\left(\frac{u_\infty D^i}{r}\right)^{1/2} = e\, n_\infty \lambda_D{}^2 D^i J$$

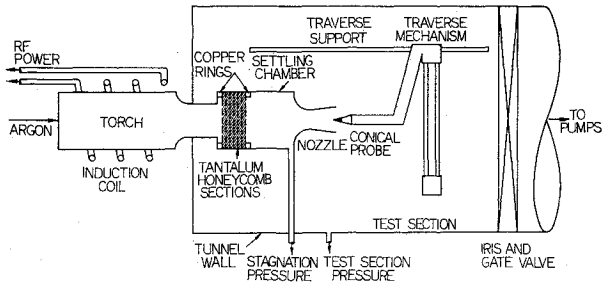

Fig. 2 Apparatus schematic.

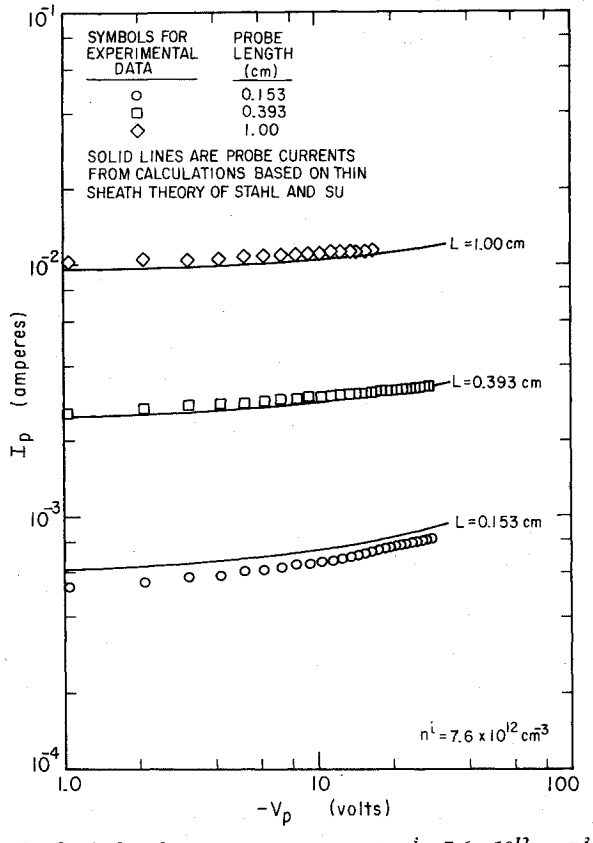

Fig. 3 Conical probe current measurements, $n^i = 7.6 \times 10^{12}$ cm.$^{-3}$.

and thus

$$I_p = \int_0^{L/\cos\theta_0} (2\pi \sin\theta_0 e\, n_\infty \lambda_D^2 D^i) Jr\, dr \qquad (5)$$

To calculate the current-voltage characteristic for a conical probe, we specify the probe voltage, and, for each value of r, we make an initial estimate of the value of θ_b, the limiting angle corresponding to the sheath outer limit and quasi-neutral region inner limit. We calculate the corresponding quantities $\bar{\eta}_b$, J, η_0 and ϕ_p using Eqs. (4), (3), (2), and (1) respectively. If ϕ_p is not equal to the probe voltage (within a specified accuracy), we make a new estimate for the value of θ_b and iterate until we obtain the specified accuracy. We then calculate the contribution to the probe current from the probe area element at r, and integrate over the probe area, Eq. (5), to find the total probe current. Then one probe voltage and its corresponding current will be known, and other voltages can be specified to determine the desired current-voltage relationship for the probe. The theoretical current-voltage characteristics are presented in Figs. 3-4 as smooth curves drawn through the calculated values. It may be observed that a modest amount of numerical effort is necessary to apply the Stahl and Su results to the interpretation of conical probe ion

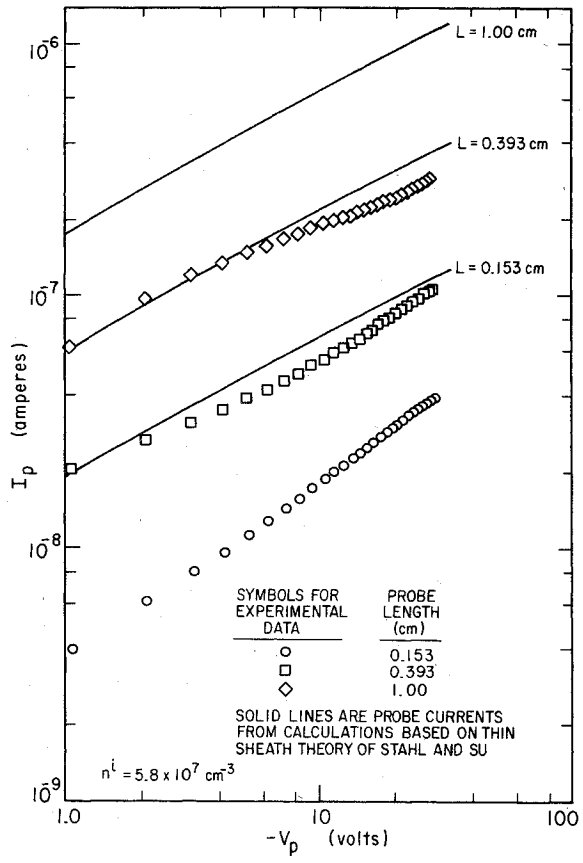

Fig. 4 Conical probe current measurements, $n^i = 5.8 \times 10^7$ cm^{-3}.

current measurements. Details of the calculations that were actually carried out for comparison with the experimental results are presented in Appendix A of Ref. 14.

Experimental Equipment

The test gas (argon) was ionized in a radio frequency induction heated torch of length 19.1 cm and diameter 7.6 cm. An argon flow rate of 0.25 g/sec and a torch power setting of 6.25 kw were selected for the experiments. The argon expanded through a converging-diverging nozzle with a 2.54 cm throat diameter and a 6.8° half-angle conical diverging contour. The 1.22 m diameter test section was maintained at low pressure by three stages of mechanical pumping and two oil booster pumps. A traverse mechanism provided positioning in axial, vertical and horizontal directions. The test set-up is shown in Fig. 2.

To obtain the large sheath sizes required for the experiments, deionization of the flow by surface recombination was employed to decrease the ion density by several orders of magnitude. A water-cooled copper chamber 7.6 cm in diameter and 10.2 cm long was added to the flow path between the torch exit and the nozzle. Placed inside this chamber were honeycomb sections 0.5 cm long with 1.3 mm square holes through them, fabricated from 0.13 mm thick tantalum sheet. Electrons and ions in the flow diffuse to the metal surfaces of the honeycombs as the gas passes through them. The ions recombine with electrons at the metal surfaces and return to the flow as neutral argon atoms. By adding up to six of these tantalum honeycombs the flow ionization was lowered from about 10^{13} to less than 10^8 ions/cc without greatly altering the neutral flow.

The butyl phthalate precision manometer with a least count of 1.94×10^{-3} Torr was used for pressure measurements. Static pressure taps were located in the wall of the copper deionization chamber (downstream of the tantalum honeycombs and just upstream of the converging section) and

Table 1 Flow conditions for conical probe measurements[a]

Number of Honeycombs	$T_0(K)$	M_∞	Re_∞/cm[b]	$T_\infty(K)$	$T^e(K)$	$T^e(eV)$	$n_\infty{}^i(\text{cm}^{-3})$
0	1480	2.15	63	582	1380	0.119	7.6×10^{12}
1	1030	2.15	99	405	1100	0.095	1.3×10^{10}
2	1080	2.15	94	425	650	0.056	2.3×10^{9}
3	900	2.16	117	352	430	0.037	9.5×10^{8}
4	820	2.17	132	319	370	0.031	4.2×10^{8}
5	730	2.17	157	284	300	0.026	1.2×10^{8}
6	675	2.17	173	263	270	0.023	5.8×10^{7}

[a] $p_0 = 1363$ cts oil $= 2.62$ torr; $L_p = 0.153, 0.393, 1.00$ cm.

[b] The Reynolds number is based on an argon kinematic viscosity determined from the expression

$$\nu_\infty \left(\frac{cm^2}{\text{sec}}\right) = \frac{\mu}{\rho} = (0.0225)\,\frac{T_\infty(K)^{3/2}}{p_\infty(\text{torr})\,\Omega^{(2,2)^*}}$$

where $\Omega^{(2,2)^*}$ is the value of the Leonard-Jones potential integral taken from Hirschfelder et al.[28]

in the wall of the test section. Impact pressure probes were mounted on the traverse mechanism. Each pressure measuring site was connected through valves and copper tubing to the manometer.

A variety of electrostatic probes was used for the experimental work. Cylindrical single and double probes were made from 0.038 cm diam tungsten wire. A small spherical probe (0.54 mm diam) was constructed using 0.008 cm diameter copper wire. Three 15° half-angle conical probes were designed and built for this study. They were copper, with lengths (from cone tip to base along the axis) 0.153 cm, 0.393 cm, and 1.00 cm, measured with a microscope. The nose radii were 1.1, 2.0 and 0.5% of the probe lengths, respectively. The base of each probe was extended conically with boron nitride electrical insulation to a 1.27 cm diam cylinder.

The voltage supply for the elctrostatic probes was a 45 v battery pack with a 10 kΩ potentiometer. Keithley Model 600A electrometers measured the probe current and voltage with respect to the tunnel wall. The electrometer outputs were fed to an *x-y* recorder to give current-voltage curves. For the spherical probe potential measurements an oscilloscope differential amplifier was used. The experimental equipment is described in more detail in Ref. 14.

Flow Calibration

Seven different flow conditions were established for conical probe measurements. Each condition was characterized by the number of tantalum honeycomb sections (0-6) placed in the deionization chamber. The measured conditions are listed in Table 1. The methods used to determine those flow conditions are explained following.

Neutral Flow Properties

A chromel-alumel thermocouple in the settling chamber measured the stagnation temperature at the flow axis upstream of the converging nozzle. The measured values of stagnation temperature were corrected for thermal radiation losses to the surrounding cooled chamber.

The stagnation pressures of all the flows were maintained at 2.62 Torr (±0.2%) as measured in the deionization chamber. Radial and axial surveys of impact pressure were made with 0.64 cm and 1.91 cm o.d. open-ended probes. Corrections were made for viscous effects[15] and shock standoff distances.[16]

The neutral flow properties at the nozzle exit were determined from the measured impact pressure, stagnation temperature and stagnation pressure using the tables of Mueller,[17] assuming an ideal gas with isentropic expansion through the nozzle.

Charged-Particle Properties

The electron temperature for the two highest ion density conditions (no honeycomb and one honeycomb) were measured with the double cylindrical probe using the method of Johnson and Malter.[18] Collisional corrections to the electron temperature measurements were negligible.

Collisional effects were present in the single probe measurements used to obtain the ion density in the flow. The ion density was therefore calculated from the single cylindrical probe ion current using the mixing formula of Thornton.[19] For lower values of ion density, the theory of Laframboise[20] as presented by Sonin[21] was used to determine the collisionless current required by the Thornton formula. But at the highest ion density (no honeycomb) the cold ion theory of Allen, Boyd, and Reynolds[22] (as applied to the cylinder by Chen[23]) was used to calculate the collisionless current. We now believe that although λ_{in}/r_p may be large, when $(\lambda_{ii}/r_p) \ll 1$ the aligned probe current increases from that predicted by Laframboise to that predicted by Chen. (For further discussion of this effect see Ref. 24.)

Thus the ion densities and electron temperatures of the two highest ion density flows were determined. But at lower ion densities (2-6 honeycombs) the double-probe ion current had no well-defined saturation, and the logarithm of the single-probe electron retarding field current plotted against probe voltage did not yield a straight line. Thus the direct measurement of electron temperature was impossible by conventional methods. Under these conditions, an approximate calculation (Appendix B, Ref. 14), using an electron energy balance together with the measured cylindrical probe currents in an iterative scheme, was employed to determine the electron temperatures and ion densities of the flows.

For the intermediate flow conditions (2-4 honeycombs) the estimated uncertainties in electron temperatures and ion densities were 15% and 4% respectively. Uncertainties in the values for the extreme flow conditions were smaller either because the values could be measured directly or because the electron and neutral atom temperatures were nearly equal.

Results

Each of the three conical probes, with respective lengths $L = 0.153$, 0.393, and 1.00 cm, was centered with its tip at the nozzle exit in the flows with measured properties listed in Table 1. The applied probe voltage of each was varied from the floating potential to about −30 v with respect to the tunnel wall. For each flow condition the current was plotted as a function of applied voltage at least twelve times on the *x-y* recorder. Values were scaled from the plots, and the average

current and experimental standard deviation were calculated at regular intervals of voltage. The characteristics were quite reproducible – the average sample standard deviation was less than 2%.

The averages of the measured currents at each voltage are presented as data points in Figs. 3 and 4. Figure 3 presents the data obtained at the highest value of $n_\infty{}^i$ (no honeycomb), whereas Fig. 4 shows the data obtained at the lowest value of $n_\infty{}^i$ (6 honeycombs). Data for intermediate values of $n_\infty{}^i$, as listed in Table 1, followed a systematic trend, and fell intermediate to those shown in Figs. 3 and 4. Data for all of the values of $n_\infty{}^i$ are plotted in Ref. 14.

For the highest ion density (Fig. 3), the probe measurements show good agreement with the calculations based on the thin-sheath theory of Stahl and Su. Even for the lowest ion density flow (Fig. 4) where the current is systematically overestimated, the theoretical curves model the slopes of the characteristics very well. For this case (as well as the intermediate cases not shown) the disagreement between the experimental and theoretical values is not surprising because the assumption in the theory that the sheath size is smaller than the distance along the probe surface is not satisfied in the calculations for $n_\infty{}^i \leq 1.3 \times 10^{10}$ cm^{-3}. It was characteristic of all of the data, as typified by Figs. 3 and 4, that the slopes of the log-log plots of current versus voltage increased for decreasing values of $L_p/\lambda_{D\infty}$ and increasingly negative values of the probe potential.

For three points of each measured current-voltage characteristics, chosen to be $-eV_p/kT^e = 25$, 100, and 250, the measured dimensionless ion densities $D_\infty{}^i L_p/u_\infty \lambda_{D\infty}^2$ ($n_\infty{}^i$ is contained in the term $\lambda_{D\infty}{}^{-2}$) are shown in Fig. 5 as functions of the corresponding dimensionless conical probe currents,

$$\frac{I_p}{n_\infty{}^i e u_\infty A_p} \frac{L_p{}^2}{\lambda_{D_\infty}{}^2} \left(\frac{\nu_\infty}{u_\infty L_p} \right) \times \left(- \frac{KT^e}{eV_p} \right)^{1/2}$$

The largest estimated uncertainties in $D_\infty{}^i L_p/u_\infty \lambda_{D\infty}^2$ (about 20%) occur at intermediate values of this parameter due to uncertainties in T^e and n^i. The nondimensionalization for the current, which was suggested by Baum and Denison,[9] was found to give the best correlation for all of the data.

For the data presented in this fashion an interesting comparison between experiment and theory can be made using the results of Chung and Blankenship[7] and Denison.[8] In both these analyses the freestream ion density could be related to the conical probe ion current in terms of an expression of the following form:

$$\frac{D_\infty{}^i L_p}{u_\infty \lambda_{D_\infty}{}^2} = C \frac{I_p}{n_\infty{}^i e u A_p} \frac{L_p{}^2}{\lambda_{D_\infty}{}^2} \left(\frac{\nu_\infty}{u_\infty L_p} \right)^{1/2} \times \left(- \frac{eV_p}{kT^e} \right)^{-1/2}$$

where, in the work of Chung and Blankenship,

$$C = (0.304)\eta \left(\frac{u_\infty}{u_c} \frac{L_s}{L_p} \frac{\nu_c}{\nu_\infty} \right)^{1/2} \frac{D_\infty{}^i}{D_c{}^i} \frac{n_\infty{}^i}{n_c{}^i} \left(- \frac{eV_p}{kT^e} \right)^{1/2}$$

and, in Denison's work

$$C = (0.508) \left(\frac{u_\infty}{u_c} \frac{L_s}{L_p} \frac{\nu_c}{\nu_\infty} \right)^{1/2} \frac{D_\infty{}^i}{D_c{}^i} \frac{n_\infty{}^i}{n_c{}^i} \left(- \frac{eV_p}{kT^e} \right)^{1/2}$$

The values of the ion diffusion coefficient were calculated according to the formula given by Kirchhoff,[25] and the ratios of freestream ion density to the boundary layer edge ion density were taken to be the same as the ratios for neutral gas densities with $\gamma = 5/3$.

For a given probe current and voltage, the Chung and Blankenship value for $(D_\infty{}^i L_p/u_\infty \lambda_{D\infty}^2)$ is larger than that of Denison by a factor of about 1.5 if we take the value of η at the boundary layer edge to be $5/\sqrt{3}$ (where the flow velocity is within 0.01% of the inviscid surface flow velocity, a somewhat arbitrary choice).

It may be observed that in these theories $(D_\infty{}^i L_p/u_\infty \lambda_{D_\infty}{}^2)$ is in fact independent of probe potential. (They assume ion current saturation to simplify their results.) However, the theories are cast in the above form in order to be consistent with the nondimensionalization used in Fig. 5. If we had followed strictly the results of the theories by removing the probe potential dependence from the abscissa, the measured data at the lower ion densities would not have collapsed into such a thin band, but the data at the highest ion density, in which saturation of the ion currents was observed, would have been correlated very well. In effect, by using the nondimensionalization of Fig. 5 we have shown that good correlation can be obtained by assuming the probe current is proportional to the square root of probe potential for most of the ion densities measured, rather than independent of probe potential, as predicted by the thin sheath theories. Correlation of probe current with the square-root of probe potential has been observed by Scharfman and Hammitt[26] and Boyer and Touryan.[27]

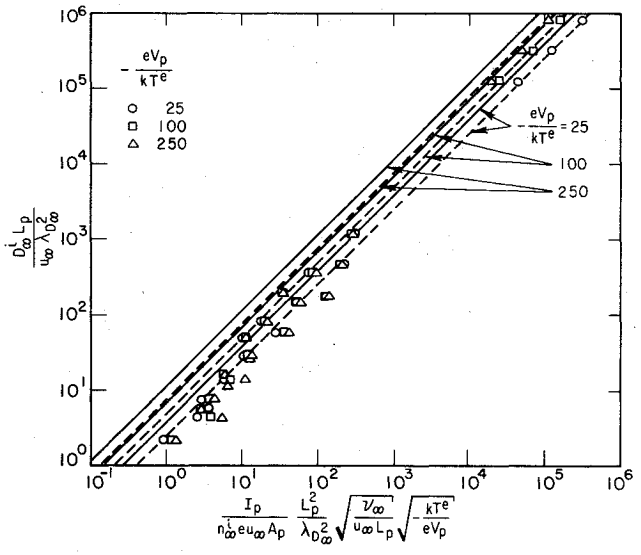

Fig. 5 Data compared with modified thin sheath theories of Chung and Blankenship (solid lines), and Denison (dashed lines).

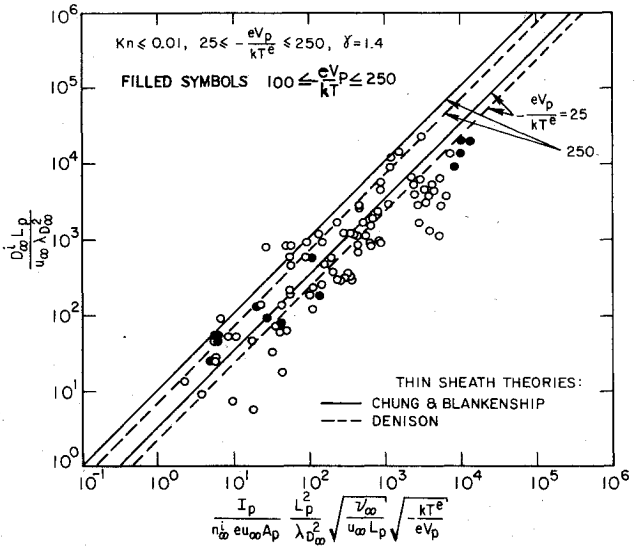

Fig. 6 Data from Scharfman and Hammitt.

Figure 6 presents the conical probe, shock tube data of Scharfman and Hammitt[26] over the same range of probe potentials, $25 \leq -eV_p/kT^e \leq 250$. These data are consistent with the thin sheath theories, but the scatter in the data is too great to permit definitive comparisons with the theories. According to the authors the scatter is due mainly to uncertainties in the measurement of electron and ion concentrations, and to spatial and temporal nonuniformities in these quantities.

The experimental data of the present study are compared to the thick-sheath theory of Hammitt[4] in Fig. 7. It is clear that the present data are not correlated very well by the parameters of Hammitt's theory. The data are also compared to the thick-sheath boundary layer theory of Baum and Denison[9] in Fig. 8. (The comparison is not completely accurate since Baum and Denison carried out their calculations for a $M_\infty = 3$ flow of a $\gamma = 1.4$ gas, whereas the present measurements were at $M_\infty \approx 2$ and for $\gamma = 1.67$. We also use T^e as the reference temperature rather than T^i_∞.) The data follow the predicted decrease in $J(Sc^i/-\phi^*)^{1/2}$ for increasing ξ/Sc^i with the theoretical ordinate a factor of two larger than the measurements for lower values of ξ/Sc^i and excellent agreement for higher values. This agreement is clearly better than that of the Hammitt theory (note the linear scale for $J(Sc^i/-\phi^*)^{1/2}$).

For overall data correlation the thin-sheath theories of Chung and Blankenship and Denison are clearly superior to the available thick-sheath theories if the data are related to the thin-sheath theories, as is done in Fig. 5. Moreover, these theories yield explicit expressions for ion number density from probe current measurements. However, like the Hammitt and Baum and Denison theories, they do not yield any current-voltage dependence such as is provided by the Stahl and Su theory.

The relative success of the thin-sheath theories in predicting the ion current collected by the cone even under conditions where the assumptions on which these theories are based are clearly violated, suggests that the sheath may remain approximately one-dimensional even when its thickness exceeds the local cone radius. An experiment was designed to test this conjecture, by carrying out measurements of the local perturbation in plasma potential in the vicinity of the cone caused by the application of a negative potential to the cone. The tests were carried out for the largest cone, $L_p = 1.00$ cm, using the small spherical probe described earlier for the local measurements. The procedure used was to measure the difference between the potential of a spherical probe positioned at a fixed point in the flow outside the domain of influence of the conical probe, and a similar spherical probe that was traversed throughout the region of influence of the cone. In this way relative changes in plasma potential in the vicinity of the cone due to changes in cone voltage could be measured. This procedure was carried out for a number of cone probe voltages, between -5 and -30 v.

The electric potentials measured with the small spherical probe in the vicinity of the large conical probe for the case $V_c = -30$, $n_{i\infty} = 3.7 \times 10^8$ cm^{-3} are shown in Fig. 9. The change in potential of the 0.54 mm diameter spherical probe was measured for the above cone voltages in radial surveys (of 0.06 cm steps) at nine axial positions (every 0.25 cm) near the cone. The direct measurements were then interpolated to obtain the points of equal change in spherical probe potential shown in the figure.

When the sphere contacted the conical probe surface its voltage assumed the value applied to the cone, but when it was within a sphere diameter of the cone, its potential change was smaller than that measured at larger radii. This behavior may have been caused by interference—the sphere may have disturbed the flow in its vicinity enough to affect the measurements. Only the measurements several sphere diameters from the cone were considered to be valid.

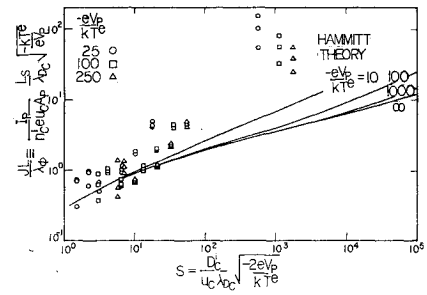

Fig. 7 Measured data compared to Hammitt theory.

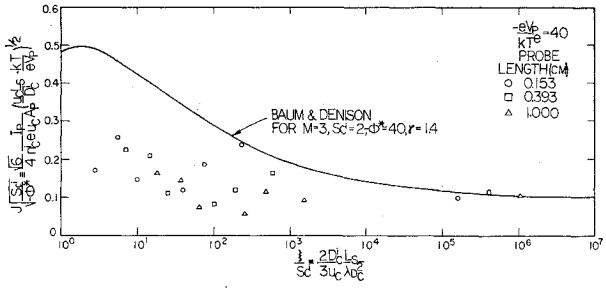

Fig. 8 Measured data compared to Baum and Denison theory.

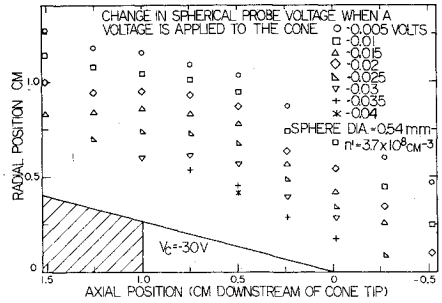

Fig. 9 Electric potential near ion attracting cone.

The measured points of equal potential lie roughly parallel to the cone surface, with only a gradual curving toward the axis at the conductor-insulator interface and upstream of the cone tip. Most of the drop from the plasma potential to the cone surface potential occured too near to the cone to be resolved by the 0.54 mm spherical probe. But as a more negative conical probe voltage was applied, the influence of the cone voltage on the potential extended further out into the flow. The near parallelism of the equipotentials and the cone surface may explain why the boundary layer type approximation for the electric potential in the thin-sheath theories yields useful results.

Conclusions

Partially ionized argon flows were produced in the laboratory to study the use of conical electrostatic probes for measurement of ion number densities over a wide range. Impact pressure, stagnation pressure, and stagnation temperature measurements were used to determine the neutral flow properties. Thin cylindrical electrostatic probes aligned with the flow were used to determine the electron temperatures and ion number densities of the flows.

Conical electrostatic probes of lengths 0.153, 0.393, and 1.00 cm were placed in seven flows of differing ion density. At the highest density, $n_\infty{}^i = 7.6 \times 10^{12}$ cm^{-3}, the ion-attracting probe current-voltage characteristics agreed well with values calculated by applying the thin-sheath continuum theory of Stahl and Su to the conical configuration. From the lowest ion

density, $n_\infty{}^i = 5.8 \times 10^7$ cm^{-3}, where the sheath extends out beyond the conical shock and boundary layer, to the highest ion density, where the sheath is embedded in the boundary layer near the cone surface, the measured probe currents followed reasonably well the thin-sheath theories of Chung and Blankenship and Denison, modified to include a dependence of current on the square root of probe voltage.

References

[1] Chung, P.M., Talbot, L. and Touryan, K.J., "Electric Probes in Stationary and Flowing Plasmas: Part I: Collisionless and Transitional Probes, and Part II: Continuum Probes," *AIAA Journal,* Vol. 12, Feb. 1974, pp. 133-154.

[2] Sonin, A.A., "Theory of Ion Collection by a Supersonic Atmospheric Sounding Rocket," *Journal of Geophysical Research,* Vol. 72, Sept. 1967, p. 4547.

[3] Dukowicz, J.K., "Theory of Convection-Conduction Dominated Electrostatic Probes: Numerical Solution of the Two-Dimensional Flat Plate Problem," Cornell Aeronautical Laboratory Rept., RA-2641-Y-1, Jan. 1969; "Conical Electrostatic Probes in a Continuum Flowing Plasma," Cornell Aeronautical Laboratory Rept. AN-2755-Y-1, Jan. 1970, Buffalo, N.Y.

[4] Hammitt, A.G., "Negatively Charged Electrostatic Probes in High Density Plasma," TRW Rept. 06488-6433-RO-00, June 1970, Redondo Beach, Calif.

[5] de Boer, P.C.T., "Ion Boundary Layer on a Flat Plate," *AIAA Journal,* Vol. 11, July 1973, pp. 1012-1017.

[6] Russo, A.J. and Touryan, K.J., "Experimental and Numerical Studies of Flush Electrostatic Probes in Hypersonic Ionized Flows: II. Theory," *AIAA Journal,* Vol 10, Dec. 1972, pp. 1675-78.

[7] Chung, P.M. and Blankenship, V.D., "Approximate Analysis of an Electrostatic Probe for Electron Density Measurements on Re-Entry Vehicles," *Journal of Spacecraft,* Vol. 3, Dec. 1966, pp. 1715-1718.

[8] Denison, M.R., "Analysis of Flush Electrostatic Probes for Reentry Measurements," TRW Report 06488-6065-RO-OO, Sept. 1970, Redondo Beach, Calif.

[9] Baum, E. and Denison, M.R., "A Thick Sheath Boundary Layer Model for Conical Electrostatic Probes in a Continuum Flow," TRW Report 06488-6456-RO-00, Sept. 1970, Redondo Beach, Calif.

[10] Stahl, N. and Su, C.H., "Theory of Continuum Flush Probes," *Physics of Fluids,* Vol.14, July 1971, p. 1366.

[11] Hantzsche, W. and Wendt, H., "Die laminare Grenzschicht bei einem mit Uberschallgeschwindigkeit angestromten nichtangestellten Kreiskegel," Bericht aus dem Institut fur Gasdynamic der Luftfahrtforschungsanstalt Herman Goering, E.V. Braunschweig. *Der Deutschen Luftfahrtforschung, Jahrbuch,* 1941.

[12] Schlichting, H., *Boundary Layer Theory,* 6th Ed., McGraw-Hill, San Francisco, Calif. 1968.

[13] Rosenhead, L., *Laminar Boundary Layers,* Clarendon Press, Oxford, 1966.

[14] Bruce, C.F., "Conical Electrostatic Probe Response in a Weakly Ionized Gas Flow," Rept. FM-74-5, May 1974, College of Engineering, University of California, Berkeley, Calif.

[15] Robben, F. and Talbot, L., "Calibration of Impact Probes at Low Reynolds Numbers," Report prepared for Sandia Corporation in fulfillment of Contract USAEC-SC-48-9942, 1971.

[16] Bailey, A.B. and Sims, W.H., "The Shock Shape and Shock Detachment Distance for Spheres and Flat Faced Bodies in Low-Density, Hypervelocity Argon Flow," Technical Documentary Rept., AEDC-TDR-63-21, 1963, Arnold Engineering Development Center, Tullahoma, Tenn.

[17] Mueller, J.N., "Equations, Tables, and Figures for Use in the Analysis of Helium Flow at Supersonic and Hypersonic Speeds," NACA TN 4063, 1957.

[18] Johnson, E.O. and Malter, L., "A Floating Double Probe Method for Measurements in Gas Discharges," *Physical Review,* Vol. 80, Oct. 1950, pp. 58-68.

[19] Thornton, J.A., "Comparison of Theory and Experiment for Ion Collection by Spherical and Cylindrical Probes in a Collisional Plasma," *AIAA Journal,* Vol. 9, Feb. 1971, pp. 342-345.

[20] Laframboise, J.B., "Theory of Spherical and Cylindrical Langmuir Probes in a Collisionless, Maxwellian Plasma at Rest," UTIAS Rept. 100, 1966, University of Toronto, Institute of Aerospace Studies, Toronto, Canada; also in *Rarefied Gas Dynamics* (J.H. DeLeeuw, ed.), Academic Press, N.Y., Vol. II, 1966, p. 22.

[21] Sonin, A.A., "The Behavior of Free Molecule Cylindrical Langmuir Probes in Supersonic Flows, and Their Application to the Study of the Blunt Body Stagnation Layer," UTIAS Rept. 109, 1965, University of Toronto, Institute of Aerospace Studies, Toronto, Canada.

[22] Allen, J.E., Boyd, R.L.F. and Reynolds, P., "The Collection of Positive Ions by a Probe Immersed in a Plasma," Proceedings of the Physical Society, Vol. 70, B, March 1957, pp. 297-304.

[23] Chen, F.F., "Numerical Computations for Ion Probe Characteristics in a Collisionless Plasma," Plasma Physics *(Journal of Nuclear Energy, c)*Vol. 7, 1965, p. 47.

[24] Bruce, C.F. and Talbot, L., "Cylindrical Electrostatic Probes at Angles of Incidence," *AIAA Journal,* Vol. 13, Sept. 1975, pp.1236-8.

[25] Kirchhoff, R.H., "An Experimental Study of the Shock Structure in a Partially Ionized Gas," University of California, Berkeley, Calif., Aeronautical Sciences Division, Rept. AS-69-8, 1969.

[26] Scharfman, W.E. and Hammitt, A.G., "Experimental Determination of the Characteristics of Negatively Charged Conical Electrostatic Probes in a Supersonic Flow," TRW Report 06488-6457-RO-00, Sept. 1970, Redondo Beach, Calif., also *AIAA Journal,* Vol. 10, April 1972, pp. 434-439.

[27] Boyer, D.W. and Touryan, K.J., "Experimental and Numerical Studies of Flush Electrostatic Probes in Hypersonic Ionized Flows: I. Experiment," *AIAA Journal,* Vol. 10, Dec. 1972, pp. 1667-1674.

[28] Hirschfelder, J.O., Curtiss, C.R. and Bird, R.B., *Molecular Theory of Gases and Liquids,* Wiley Inc., N.Y., 1954.